Chapter 3

Waveform Design for MIMO Radar and SAR Application

Stéphane Méric and Jean-Yves Baudais

Additional information is available at the end of the chapter

http://dx.doi.org/10.5772/intechopen.71300

Abstract

Remote sensing applications using radar systems require specific signal processing to obtain high resolution for radar imagery. This high resolution is essential in detection and imaging processing and is provided by using synthetic aperture radar (SAR) processing. This chapter describes the application of the multiple-input multiple-output (MIMO) configuration and the orthogonal frequency-division multiplexing (OFDM) concept to overcome some existing limitations with conventional imaging systems as well as to assess the improvements achieved.

Keywords: remote sensing, synthetic aperture radar (SAR), multiple-input multiple-output (MIMO) SAR, orthogonal frequency-division multiplexing (OFDM) SAR, waveform design

1. Introduction

Nowadays, airborne or satellite systems are essential for monitoring and observing the evolution of the Earth. Radar imaging systems make this observation possible through acquiring various information about observed regions. A radar system illuminates a region by transmitting electromagnetic waves at different frequency bands, such as L, S, C or X ones, and this system receives the diffused waves from this region in monostatic configuration. In the case of bistatic configuration, the receiving system is located at another place of the transmitting one. In case of monostatic, one of the greatest advances in radar imaging is the principle of aperture synthesis from a moving radar system in order to obtain high-resolution images. This technique is widely known as synthetic aperture radar (SAR). A SAR system provides required data for different applications such as polarimetry, interferometry and tomography. These techniques make it possible to collect various information about the region of interest. Thus, we can retrieve intrinsic characteristics such as soil properties (roughness, moisture), vegetation information (type of vegetation and height of vegetation) or urban density. However, radar imaging techniques are dependent on the characteristics of the SAR imaging system.

Among other parameters, capabilities to obtain the information of the region of interest depend on the spatial resolutions of the imaging system and the global signal-to-noise ratio (SNR). Actually, high resolution for a radar system is essential for detection and image processing and a high SNR is the first condition to achieve good spatial resolutions. Specific geometric configurations and signal processing provide opportunities to reach high spatial resolutions and to enhance system performances. This chapter describes the application of the multiple-input multiple-output (MIMO) configuration and the orthogonal frequency-division multiplexing (OFDM) concept to overcome some existing limitations with conventional imaging systems. Moreover, we propose how to assess the achieved improvements.

The chapter is divided into three sections. In Section 2, we briefly explain the basic characteristics of a radar imaging system and the signal processing applied to obtain radar images. This introduction is important to exhibit the challenges of the MIMO configuration and the OFDM concept. We describe the steps providing a SAR image and the corresponding paragraph deals with the description of a radar system and the respected geometric configuration. The SAR signal processing is also addressed to describe the SAR image characteristics. In Section 3, we present the MIMO configuration. The MIMO principle is based on several transmitting antennas and several receiving antennas. This transmission/reception configuration is widely used in digital communication applications. For radar applications, this kind of configuration leads to numerous improvements such as moving target identification or radar resolutions. In this section, we synthesise the different approaches of the MIMO radar in a colocalised configuration and we describe the SAR processing relied on. Also, we present different opportunities to exploit the spatial diversity given by the MIMO radar. We evaluate performances of different methods by analysing the effect of the SAR resolution and the noise robustness. The processing assessment is essentially based on the peak sidelobe ratio (PSLR) and the integrated sidelobe ratio (ISLR). Finally, some examples through simulations (basic system and operating spaceborne system) and measurements (ground-based SAR system) are provided to illustrate our developments. Section 4 deals with the OFDM signal. For digital communications, OFDM signals have shown many advantages such as the allocated bandwidth optimisation or the robustness against impulsive noise. For radar applications, using OFDM signals is essential in context of MIMO radar to reach the transmitted signal orthogonality. In this section, we present the use of OFDM signals for SAR imagery by describing OFDM single-input single-output (SISO) SAR configuration. Moreover, we propose to illustrate the range ambiguity in radar images and the way to remove the unexpected phenomena. Thus, we design OFDM radar signals to reduce range ambiguity in SAR images based on radar image parameter such as PSLR and ISLR. At the end of this section, we give examples through simulations (basic system and operating spaceborne radar). Finally, we combine OFDM waveforms and the MIMO configuration to achieve a SAR image in Section 5. Section 6 concludes this chapter.

2. SAR processing

The SAR technique is well-known as a high spatial resolution signal processing. In other words, this technique makes possible to obtain resolutions in range and azimuth of the radar

image less than around 30 cm in both dimensions [1]. This method is based on the signal focusing both along range axis and azimuth axis. The high resolution in range is obtained by using the properties of the transmitted signal and especially the bandwidth of this signal. Along the azimuth axis, the high resolution is related to the combination of different signals received at different times that induces the radar sensor to move along the azimuth axis. We propose to deal with the SAR processing with respect to the performances we address in this chapter. In our case, these performances are relied to SAR image characteristics such as range ambiguity and radar image resolutions. The radar signal processing is the way to reach these requested SAR image characteristics. Moreover, these image characteristics are based on the radar geometric configuration.

2.1. Radar geometric configuration

Let us consider the geometric configuration described in **Figure 1**. The geometry related to the radar sensor is partially described by the antenna aperture angles both in elevation β_e and azimuth β_{az}. These angles determine the footprint of the radar. On the one hand, the angle β_e determines the swath width W_s of the radar along the range axis and the elevation angle α_e aligns the illuminated area away the azimuth axis with respect to the height H of the radar sensor. On the other hand, the angle β_{az} determines the azimuth swath width W_{az}. The distance and azimuth swath widths determine the maximum observation distances of the radar along these dimensions. The single ground scatterer n is located on the illuminated area at the coordinates $\left(x_{sol\_n}, y_{sol\_n}\right)$ with respect to the range-azimuth plane. When the radar imaging process is applied, the region of interest is imaged regarding the line-of-sight (slant). Consequently, the image of the ground scatterer n located on the ground is then projected onto this axis of sight and is depicted with the coordinates $\left(x_n, y_n\right)$ in the slant-azimuth area. The following descriptions deal with SAR images, which are referenced in the slant-azimuth area unless otherwise specified. The transformation from the slant-azimuth area to the range-azimuth area is carried out by means of a projection of the ground plane onto the slant plane.

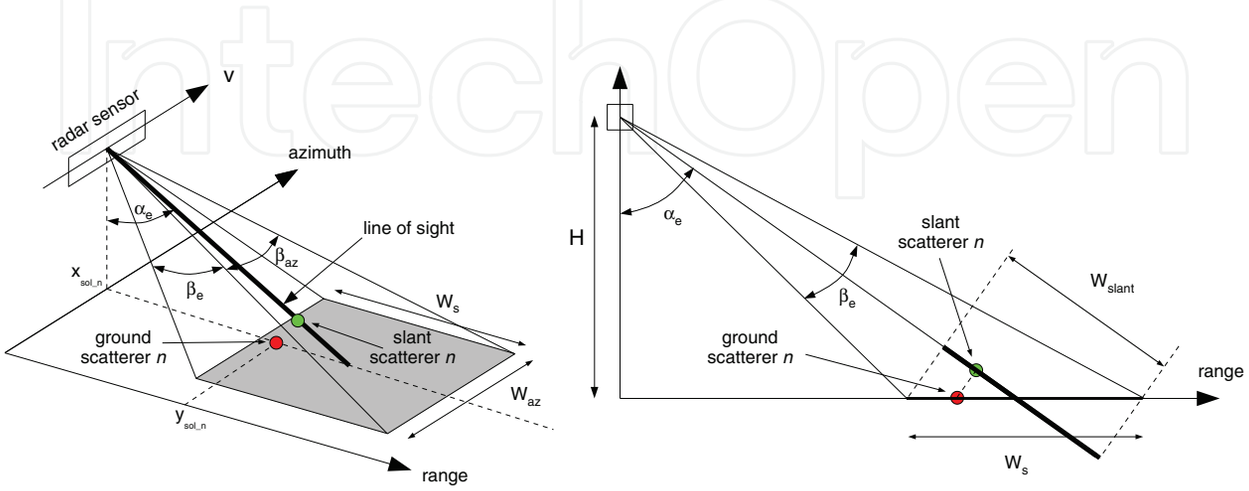

Figure 1. SAR geometric configuration.

2.2. SAR signal processing

As mentioned before, the spatial resolutions δ_{az} along the azimuth axis and δ_{rg} along the range axis require a transmitted bandwidth B and a radar motion v. The considered geometric configuration (see **Figure 1**) is that of a stripmap radar image. The elements we describe are useful in the following sections to deal with MIMO configurations and waveform design.

2.2.1. Pulse compression

The transmitted signal is $s_e(t)$ as a frequency-modulated periodic signal (chirp) of magnitude A_0 and having a bandwidth B centred around the carrier frequency f_c. This signal is defined with

$$s_e(t) = A_0 \,\mathrm{rect}\left(\frac{t}{T_p}\right) \exp\left(i2\pi\left(f_c t + Kt^2\right)\right) \tag{1}$$

where $\mathrm{rect}\left(t/T_p\right)$ is the rectangular window of T_p duration and K is the frequency slope of the chirp, that is, $K = B/T_p$. Finally, the signal $s_e(t)$ is transmitted with a rate of pulse repetition frequency (PRF), which is considered to be much lower than $1/T_p$. Considering a single ground scatterer located at a distance R away from the radar and characterised with a radar cross section (RCS) σ, the received signal obtained after a matched filter processing based on the transmitted signal (Eq. (1)) is given by

$$s_{rc}(t) = A\sigma T_p \exp\left(-i\Phi\right) \mathrm{sinc}\left[KT_p\left(t - \frac{2R}{c}\right)\right] \exp\left[i2\pi f_c\left(t - \frac{2R}{c}\right)\right] \tag{2}$$

where $\Phi = \pi B\left(t - \frac{2R}{c}\right)$ and the coefficient A includes all the propagation losses and the other elements involved in the radar equation. We can deduce the range resolution related to the mainlobe width of the sinc function in Eq. (2) with

$$\delta_{rg} = \frac{c}{2B} \tag{3}$$

It is worth to notice the influence of the bandwidth B on the SNR of the radar sensor [2]. Actually, if we consider P_t as the transmitted power (in our case, $P_t = \mathrm{PRF}\ \ T_P A_0^2/2$) before pulse compression through G_a (the antenna gain) and for the wavelength $\lambda_c = c/f_c$, the SNR after matched filtering by the radar sensor is described with

$$\mathrm{SNR} = \frac{P_t G_a^2 \lambda_c^2 \sigma}{(4\pi)^3 R^4 P_n} B T_p \tag{4}$$

Because the noise is uncorrelated to the transmitted pulse, the noise power is not modified by the pulse compression processing contrary to the transmitted signal involved in the pulse compression processing, which is amplified by a factor BT_p.

2.2.2. Synthetic aperture along azimuth axis

In this work, we use the backprojection algorithm to focus the reflected signals acquired along the moving path of the radar. In the slant-range plane, the geometric configuration is reminded in **Figure 2**. The reflected signal is acquired along the azimuth path limited by the length L, which is also called the synthetic antenna length. The backprojection method is based on the temporal correlation between the theoretical response of each pixel of the final image corresponding to the coordinates (x, y) on the region of interest with the set of received signals $s_r(t, u)$ for each u position. The coordinates are calculated regarding the reference point $(X_c, 0)$. Let us consider a single point scatterer located at (x_n, y_n) coordinates. At a given u position, the received signal is then defined with

$$s_r(t,u) = A\sigma \,\mathrm{rect}\left(\frac{y_n - u}{W_{az}}\right) s_e\left(t - \frac{2R(u)}{c}, u\right) \tag{5}$$

The distance $R(u)$ varies as a function of u and is equal to $R(u) = \sqrt{x_n^2 + (y_n - u)^2}$. The rectangular window limits the visualisation of the scattering reflecting point by the radar system as a function of its u position and the y_u azimuth position of the reflector point: if $|y_n - u| > W_{az}/2$, then this point is not seen by the radar. Finally, the correlation is carried out by means of matched filters with respect to the geometric configuration. The focused image function $f(x, y)$ corresponds simultaneously to matched filter processing both along range axis and azimuth axis.

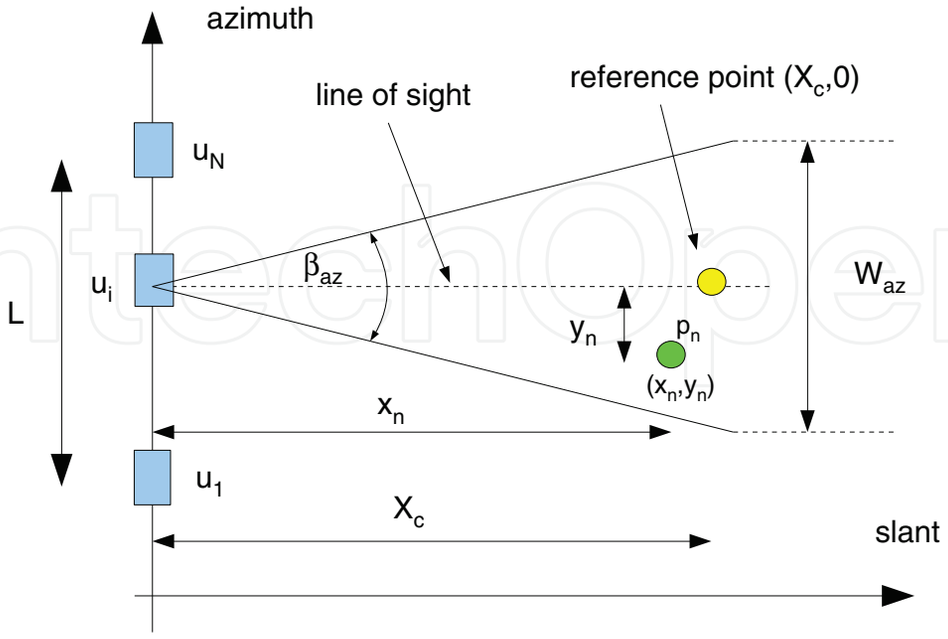

Figure 2. SAR geometric configuration in the slant-range area.

2.3. SAR image characteristics

The two-dimension matched filtering is finally given with

$$f(x,y) = \exp\left(-i2\pi f_c \frac{2x}{c}\right) \int_{y_n - W_{az}/2}^{y_n + W_{az}/2} s_{rc}(\tau(x,y),u) \exp\left(-i2\pi f_c \tau(x,y)\right) du \tag{6}$$

where $\tau(x,y) = 2R(x,y)/c$. Based on the formulation of Eq. (6), one can express the theoretical azimuth resolution δ_{az} [3]:

$$\delta_{az} = \frac{D}{2} \tag{7}$$

if the value of L is sufficient to entirely cover the area under image processing. We can note that Eq. (6) is described with respect to the delay $\tau(x,y)$ and the u position. Thus, the sampling of the range compressed signal achieves the adaptation to the $(\tau(x,y),u)$ samples by means of an oversampling operation (so-called zero-padding operation in the spectral domain) and a linear interpolation. The backprojection procedure is described in **Figure 3** and a result of this procedure is also exhibited in **Figure 3** for nine point scatterers.

Until now, the radar system is presented as an ideal one. Actually, the electromagnetic wave used to make a radar image undergoes perturbations due to different factors [2]. The first kind of disturbances affects the received power:

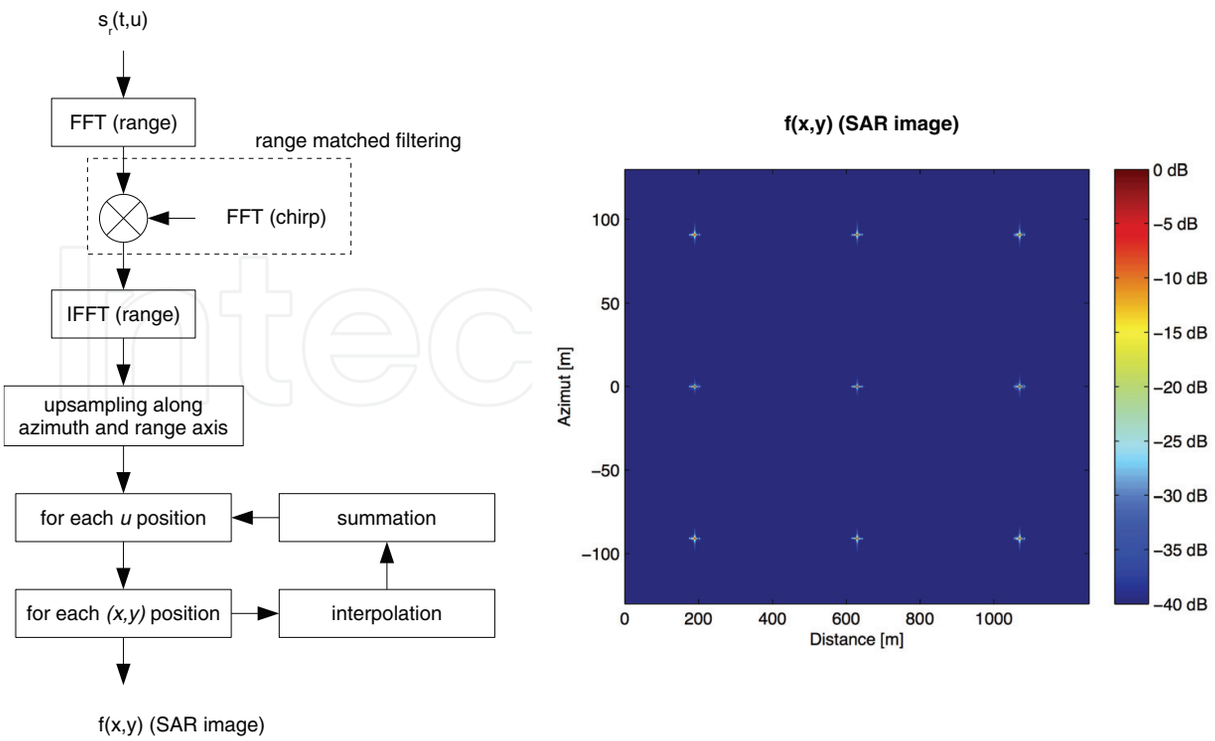

Figure 3. Backprojection procedure and nine point scatterers SAR image.

- Power loss related to the transmitter during the transportation of the transmitted signal between the signal generator and the antenna. The use of coaxial cables or waveguides implying a loss in the transmitted power compared to that generated (loss around 3 or 4 dB according to the signal characteristics, to the wavelength of the carrier, to length of the cable or of the waveguide…);
- Power loss related to the media that the electromagnetic wave run through during the transmission. The electromagnetic wave passes through different media with different attenuation and phase shift properties. As an example, in the case where the wave passes through the atmospheric medium, it suffers losses, which are expressed in dB per km. This loss is related to the interaction between the electromagnetic wave and the molecules contained in the atmosphere and depends on the carrier frequency of the transmitted wave;
- Power loss related to the receiver during the reception of the electromagnetic wave by the antenna during the transmission to the information sampling and storage components. This transfer involves losses of the same order as during transmission.

Other perturbations are possible such as:

- Noise related to on-board electronics (example of receiver noise),
- Electromagnetic waves diffused by reflectors in the area to be imaged (example of the speckle phenomenon visible on a radar image),
- Electromagnetic waves from reflectors not in the area to be imaged but creating ambiguities in range or azimuth on the radar image,
- Electromagnetic waves coming from other applications, and which disrupt the radar image interpretation (example of jammers).

The following section of this chapter mainly focus on either the different MIMO configuration to make radar system more robust against noise through the SAR processing and range ambiguities, which can be mitigated by using specific waveform design such as OFDM.

3. MIMO configuration

In this section, we present firstly the limitations regarding the SISO SAR configuration relied to the chirp waveform transmitted signal. We introduce some processing and system design solutions based on the MIMO principle, to overcome these limitations. This principle is addressed through the various radar configurations and its application to SAR imagery, called MIMO SAR. Comparing with SISO radar, we focus on the robustness of signals to noise and interference and on azimuth resolution. We describe the SNR to assess the influence of the MIMO configuration comparing to the SISO one. The SNR expression we propose is based on the lossless radar equation as described with Eq. (4). Many ways to reduce the noise influence are based on using bandpass filters [4] with low bandwidth that drives thermal noise at the receiver systems down. Other methods exist by using multiple antenna configurations as multiple-input single-output (MISO) for transmitting approach or single-input multiple-output

(SIMO) for receiving approach. In case of a complete combination (M receiving antenna and N transmitting antenna), which is the MIMO configuration, the SNR equation yields [5]:

$$\mathrm{SNR}_{\mathrm{MIMO}} = N^2 M^2 \frac{P_e G_a^2 \lambda_c^2 \sigma}{(4\pi)^3 R^4 P_n} B T_p \tag{8}$$

Thus, we notice easily that by increasing the number of transmitting and receiving antennas, we obtain an improvement of the SNR in relation to the number of antenna.

Nevertheless, concerning the problem related to radar imagery, the SNR coefficient does not make the measurement of radar image quality possible. It is therefore necessary to use other parameters, which take into account the imaged region of interest. These parameters measure the effect of disturbances on the radar image. Thus, two SAR image parameters are commonly used to assess the image quality: the so-called PSLR and ISLR. Considering a SAR image composed of discrete elements z_n, that is, the pixel, we introduce these two image quality parameters with [6]:

1. The ratio between the amplitude of the most powerful sidelobe and the amplitude of the mainlobe. This ratio is called PSLR and is expressed with:

$$\mathrm{PSLR} = \frac{\max\limits_{n \in I \setminus I_0} |z_n|^2}{\max\limits_{n \in I_0} |z_n|^2} \tag{9}$$

where $|z_n|$ is the magnitude of the pixel n in the image, I is the set of all the pixels belonging to all the image (mainlobe and secondary lobes), and I_0 is the set of the pixels belonging to the mainlobe;

2. The ratio between the energy contained in the secondary lobes and the energy in the mainlobe. This ratio is called ISLR and is formulated with:

$$\mathrm{ISLR} = \frac{\sum\limits_{n \in I \setminus I_0} |z_n|^2}{\sum\limits_{n \in I_0} |z_n|^2} \tag{10}$$

These two parameters are defined on the basis of the impulse response, that is to say by considering the presence of a single scatterer on the region of interest. In the case of the PSLR parameter, we measure the radar system capability to image scatterers having a low RCS with respect to scatterers having a much stronger RCS. Indeed, the secondary lobes associated with a scatterer having a strong RCS may mask the presence of scatterers having a much lower RCS. The PSLR parameter, thus reflects the appearance of a parasitic object on the region of interest. In the case of no artefact, the PSLR parameter value is obtained from the first secondary lobe of the impulse response related to the image of the point scatterer. In the case of ISLR, we measure the interference amount and noise located in the region of interest [7]. By taking into account the relation between the number of antenna and the SNR formulated in case of MIMO

configuration (Eq. (8)), it is therefore possible to decrease the ISLR value more efficiently than with a SIMO or a MISO configuration.

3.1. Coherent MIMO radar and SAR processing

In this paragraph, we consider a coherent MIMO radar system (C-MIMO) composed of a linear array with M transmitting antennas and a linear array of N receiving antennas (**Figure 4**). The C-MIMO means that the distance between the radar and the target is high compared to the distance between antennas. The transmitting antennas are separated from each other with a distance d_T and the receiving antennas with a distance d_R. The transmitting (receiving) antennas are close enough to each other to consider the transmitting (receiving) angles of the transmitted and received signals, respectively, equal to the same angle θ (see **Figure 4**) that means the distance of the scene far away the radar is more greater than d_R and d_T.

Moreover, each of the M antennas transmit signals $(\phi_i(t))_{i\in[1,M]}$ that are orthogonal to each other. In case of non-orthogonal waveforms, we have to design $\phi_i(t)$ signals with the lowest correlation level to each other. The SAR processing that we applied to this MIMO configuration is based on applying matched filters in range that makes it possible to separate different transmitted signal at the reception. After this step, $M \times N$ signals with a low cross-correlation level are available on which we apply matched filters in azimuth with respect to the SAR geometric configuration as described in Section 2.

The MIMO SAR system concept is widely described and different design strategies for the receiver are proposed in the literature [5, 8, 9]. The MIMO imaging procedure is mainly based on applying SAR processing (back projection or Omega-K method) on the signals available at the matched filters (range and azimuth). Also, the MIMO SAR system is made to obtain a better SNR and consequently a better robustness against noise and better resolution in azimuth with respect to the SISO configuration possible. Another strategy is the joint use of specific waveforms (rather than the chirp one) and new kind of reception filters [10, 11]. This strategy improves the PSLR and ISLR levels and therefore makes the radar system more robust.

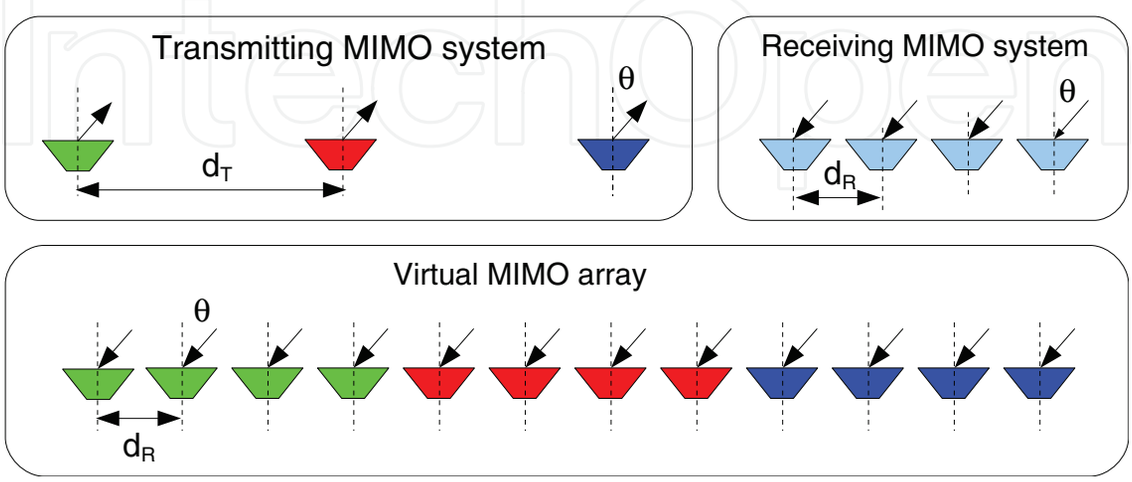

Figure 4. Uniform virtual MIMO array principle.

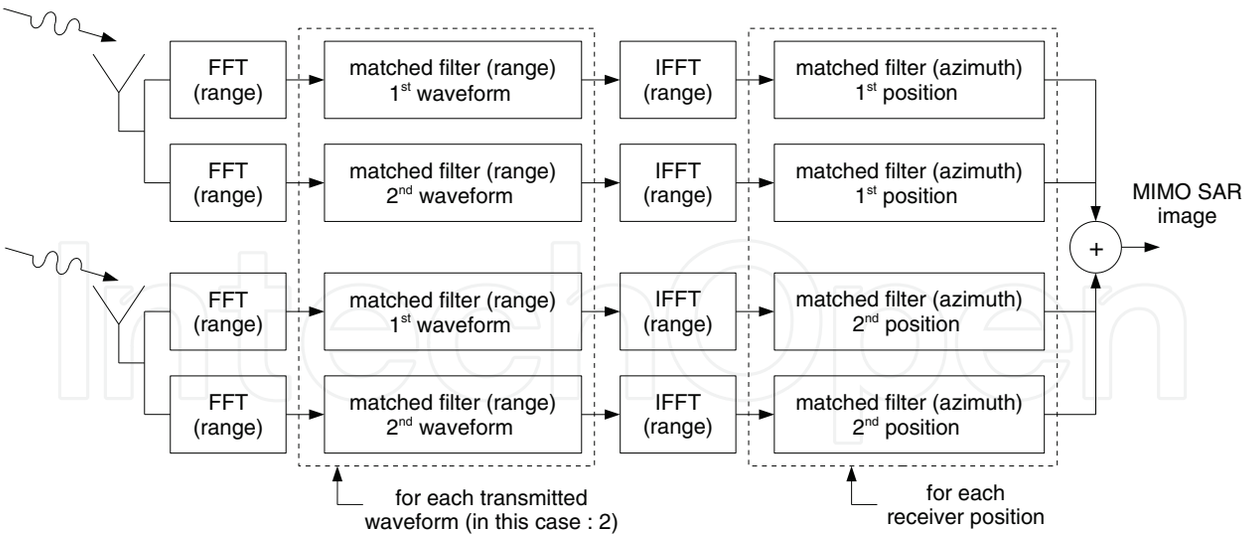

Figure 5. SAR images coherent sum.

Although many receiver designs were examined in [12], we propose to describe the results we obtain with the receiver design exhibited in **Figure 5**. The applied method uses $M \times N$ couples of transmitter and receiver combinations. For each couple, a SAR image is provided through a basic SAR processing and the final MIMO SAR image is given after a scalar sum of each SAR image.

3.2. Method assessment

To evaluate the robustness of the MIMO configuration, we compare the results we obtained for the SISO and MIMO configurations. These assessments are based on the PSLR and ISLR measurements, defined in Eqs. (9) and (10), respectively. Moreover, we extract the azimuth resolution δ_{az} by evaluating the mainlobe width at -3 dB for a point-like target respons along the azimuth axis.

3.2.1. Simulation

The geometric configuration is shown in **Figure 6**. The radar imaging system consists of two transmitting antennas and two receiving antennas. The transmitted signals are of the chirp type (up and down-modulated) whose carrier frequency f_c is 6 GHz. The bandwidth B of these chirps is 1 GHz and is centred around the carrier frequency f_c. The transmit antennas identified with (1) and (2) in **Figure 6** are spaced 1 m apart, that is, $40 \times \lambda_c/2$, and the receiving antennas identified with (3) and (4) in **Figure 6** are spaced 12 cm apart, that is, approximately $2 \times \lambda_c/2$. This configuration matches the co-located condition because the maximum range is about 2.5 m. The imaging system is located at a height $H = 2.40$ m from the ground with an incidence angle α_e of 45°. The azimuth aperture angle for each antenna is β_{az} = 54°. The point-like scatterer is located at a slant range of 4.55 m and at -0.22 m in azimuth. Finally, we consider a radar data collection along a 3 m azimuth distance (± 1.5 m). As the azimuth displacement is limited to 3 m, the considered antennas for the SISO configuration are located at position (3) and (4) in **Figure 6**

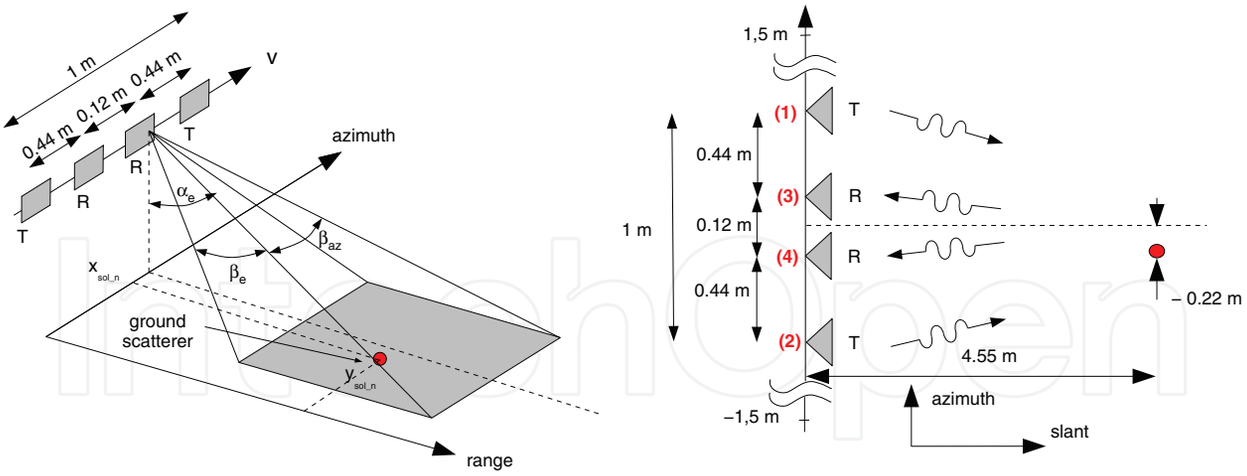

Figure 6. Geometric configuration used in simulation.

for the receiver and the transmitter, respectively. When white Gaussian noise is considered for simulations, the SNR level is set up to −30 dB at the receiving stage. Also, we have SAR images for both SISO and MIMO configurations, which are exhibited in **Figure 7**.

Moreover, the results we obtained in noisy conditions or not, for the azimuth resolution, ISLR and PSLR, are given in **Table 1**.

As a conclusion, the azimuth resolution is slightly improved for the MIMO situation that could be planned because of the coherent summation of different SAR images. Moreover, we obtained lower PSLR and ISLR levels for MIMO configuration than for the SISO one that means the better robustness of MIMO system against noise for radar imaging.

3.2.2. Measurement

The experimental system is shown in **Figure 8**.

The radar system uses a vector network analyser (VNA) transmitting a step frequency continuous waveform. The SAR processing is based on a stop & go configuration. The experimental settings match those used by the simulation: the carrier frequency is 6 GHz, the transmitted bandwidth is 1 GHz and this MIMO radar system is also composed of four antennas, which are arranged as described in **Figure 6**. In the same way, the radar scene consists of a metallic trihedral arranged on the ground to obtain the same experimental conditions described in **Figure 6**. The VNA is placed on a 3 m rail that provides the displacement to perform the SAR processing. The images provided by this experimental system are then obtained for SISO and MIMO configurations and are exhibited in **Figure 9**.

Consequently, different values for the azimuth resolution, PSLR and ISLR are obtained and shown in **Table 2**. As mentioned in Section 3.2.1, the results obtained with the experimental measurements confirm those obtained with the simulated configuration even if the values are slightly different, that is mainly due to the measurement conditions.

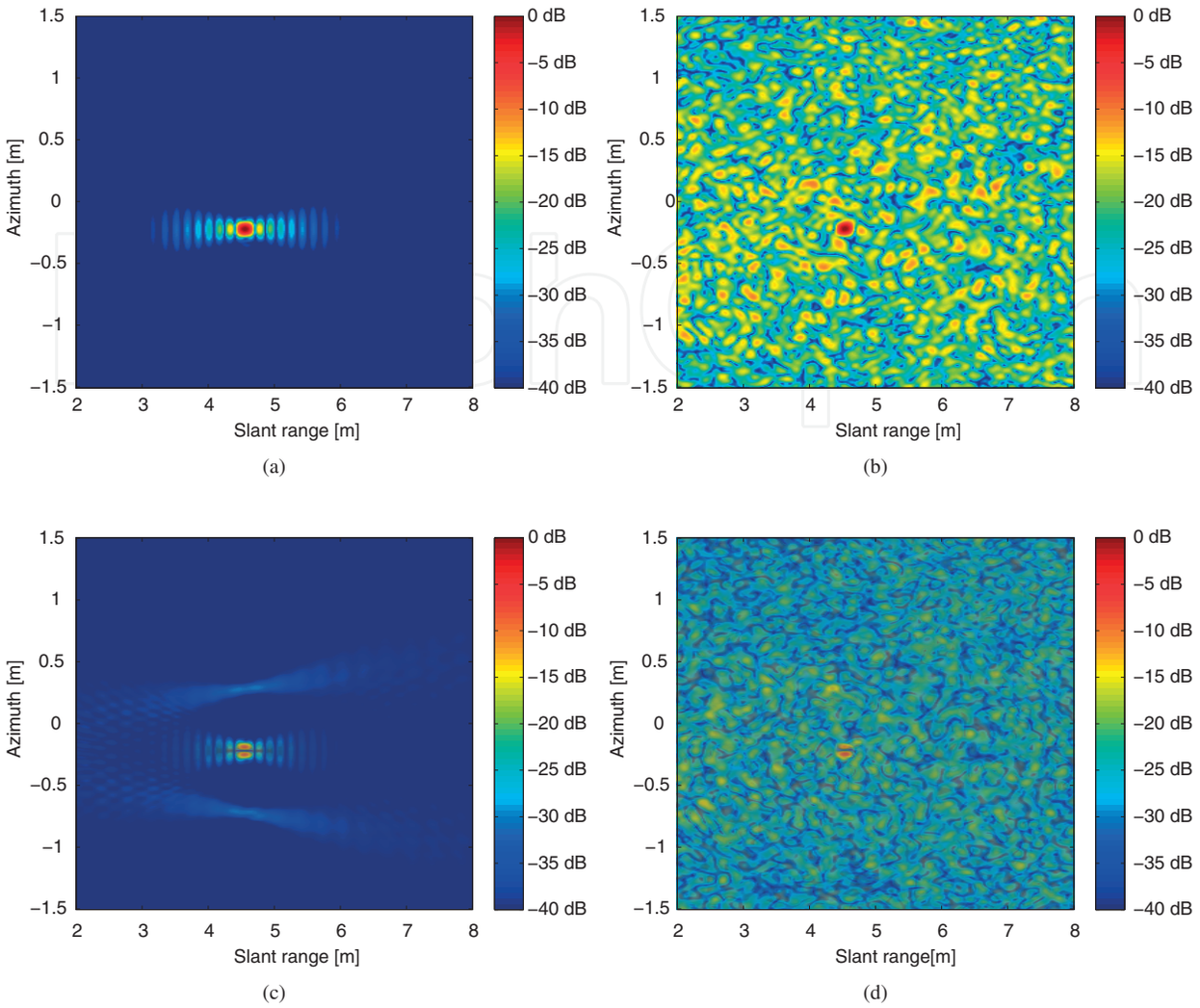

Figure 7. SISO and MIMO SAR images provided by simulation.

	Azimuth resolution (m)	PSLR (dB)	ISLR (dB)	PSLR (dB)	ISLR (dB)
		Without noise		With noise	
SISO	0.056	−13.9	−31	−9.5	−11.7
MIMO	0.048	−14.2	−31	−11.2	−14.4

Table 1. Simulation results of the azimuth resolution, PSLR and ISLR for SISO and MIMO configuration.

3.3. Discussion

Section 3 proposes an application of the MIMO principle to SAR imagery. Simulations and experimental measurements are conducted to quantify the gain we are able to obtain by using a MIMO configuration rather than a SISO one. For the given receiver design, the performance improvements are noticeable whether by simulation or by measurement. Thus, the use of the MIMO principle in SAR imagery reinforces the robustness of the radar system against noise.

Figure 8. Overview of the measurement system.

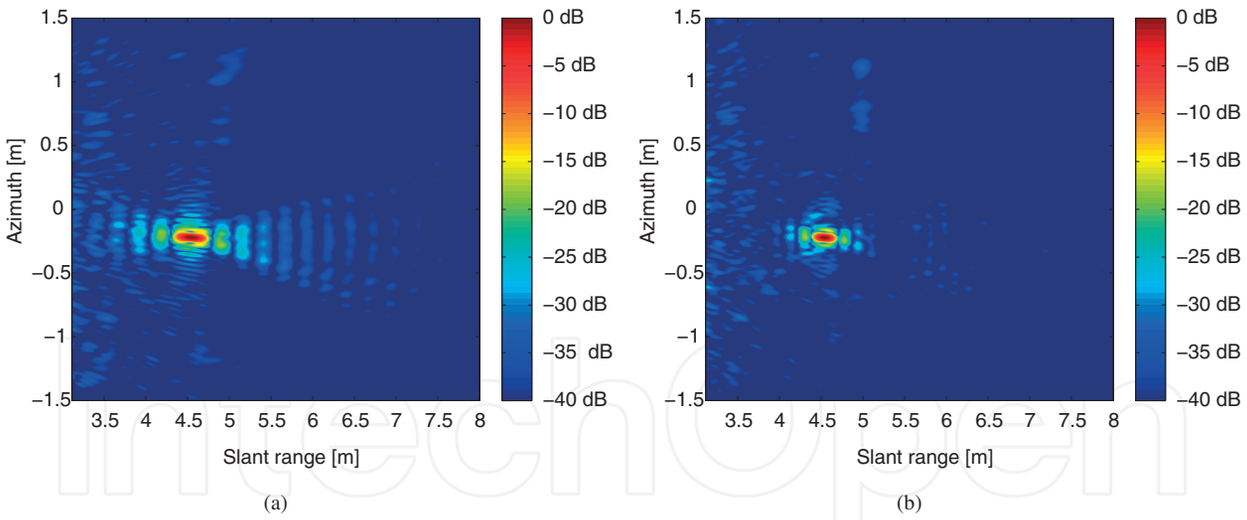

Figure 9. SISO and MIMO SAR images provided by measurements.

	Azimuth resolution [m]	**PSLR [dB]**	**ISLR [dB]**
SISO	0.043	−13.6	−31.4
MIMO	0.038	−15.3	−34.8

Table 2. Measurement results of the azimuth resolution, PSLR and ISLR for SISO and MIMO configuration.

Moreover, the MIMO principle does indeed to improve the azimuth resolution even this improvement is low and may be considered as negligible in the case of 2-by-2 MIMO configuration.

At this point, it is worth to notice that these improvements can be achieved under the orthogonal transmitted waveform condition. In this section, the up- and down-modulated chirp makes it possible to partially reach this orthogonal condition. Nevertheless, many applications require a better orthogonality criterion or need more than two transmitted waveforms. For this purpose, frequency modulation techniques are useful to get low correlation level between two signals.

4. OFDM design

The OFDM is based on frequency division multiplexing (FDM) in which subchannels overlap without interfering and with the minimal frequency spacing. It is a modulation technique widely used in wireless communication systems such as access networks, cellular networks, broadcast networks and also in wireline communication systems such as digital subscriber line (DSL) and powerline communications (PLC). With OFDM, the data are transmitted in parallel subchannel, which means that the channel distortion experienced by each subchannel decreases. The channel equalisation procedure at receiver side is then simplified with the respective complexity increase counterpart at transmitter size. With the availability of efficient software and electronic technologies, the modulation at the transmitter side is efficiently realised with the inverse fast Fourier transform (iFFT). The continuous baseband signal using N subchannels, also called subchannels, and transmitting N complex data symbols a_i is defined with

$$s_e(t) = \frac{A_0}{\sqrt{N}} \sum_{i=1}^{N} a_i \exp\left(i2\pi f_i t\right) \mathrm{rect}\left(\frac{t}{T_p}\right) \tag{11}$$

where the subchannel spacing $|f_i - f_{i+1}|$ is equal to the inverse of the symbol time length $1/T_p$. The OFDM transmission mainly consists in iFFT transform of the data a_i at the sampling time T_p/N. The data symbols are recovered with an FFT at receiver side.

One of the major benefits of OFDM transmission is the spectrum design. Holes in the spectrum can be simply created by turning off some subchannels obtained with $a_i = 0$ for the corresponding subchannel i, as shown in **Figure 10**.

This key advantage is used in waveform radar design to increase the localisation and the tracking of targets in noisy environment [13], to increase the robustness of target detection in jamming scenarios [14], to improve efficient computational performance in 2D SAR imaging scenarios [15] and the OFDM is also considered as one proper waveform for communication-radar integrated system [16]. These few examples show the potential of the OFDM waveform to meet the needs of radar and especially SAR applications.

The first capability measure of the OFDM waveform for radar application is the ambiguity function. With respect to the delay τ and the frequency Doppler ν, this ambiguity function using Eq. (11) and in the case where $f_i = \left(i - \frac{N+1}{2}\right)\frac{1}{T_p}$ is [17]

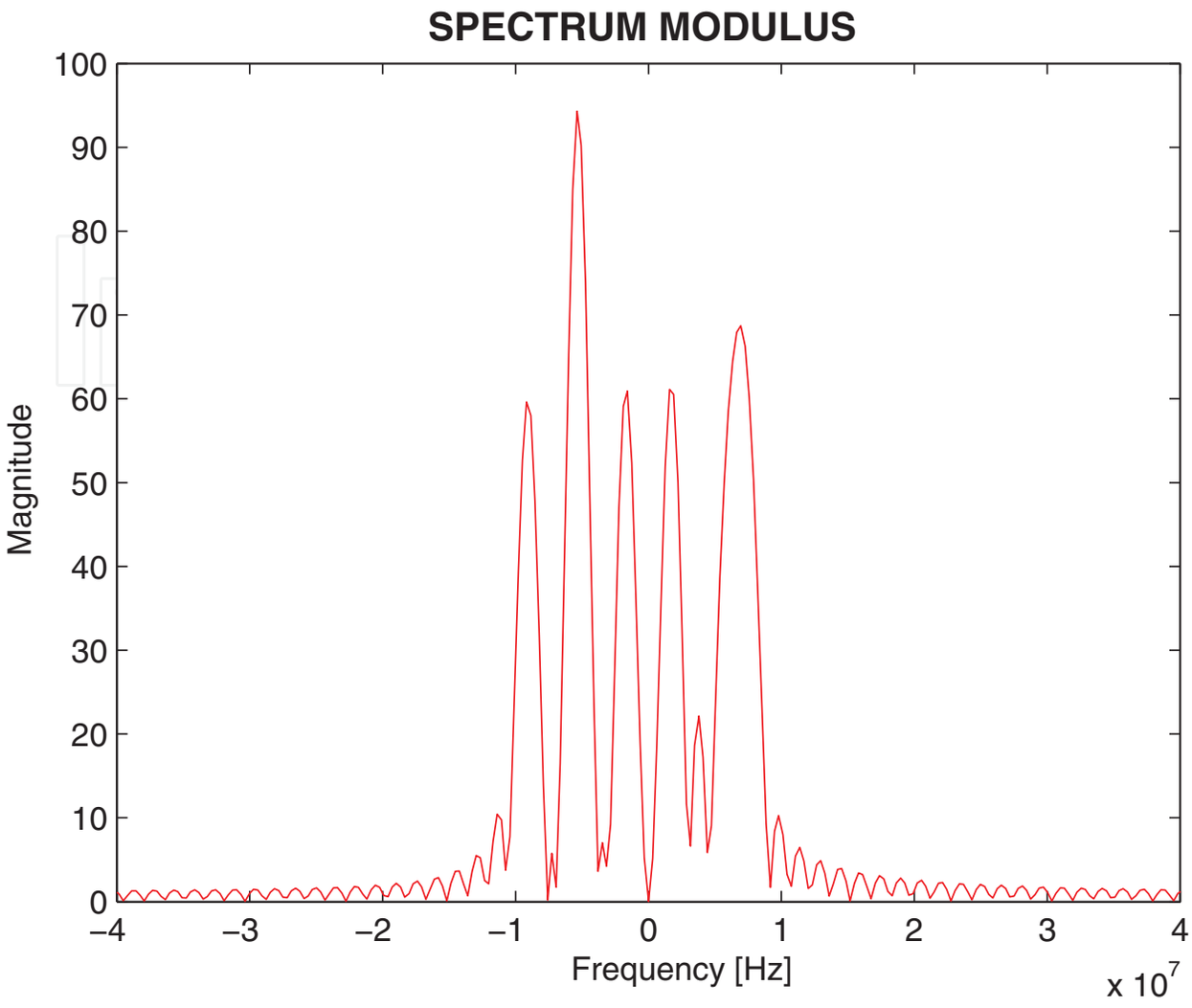

Figure 10. OFDM signal spectrum with $(a_i)_{i=1}^{13} = [1011010100110]$.

$$\chi(\tau,\nu) = \left(T_p - |\tau|\right)\frac{A_0^2}{N}\sum_{i=1}^{N}\sum_{j=1}^{N} a_i a_j^* \exp\left(i\pi\left(i-j+\nu T_p\right)\right)\exp\left(i\pi\left(i+j-N-1+\nu T_p\right)\frac{\tau}{T_p}\right) \times \operatorname{sinc}\left(\pi\left(i-j+\nu T_p\right)\frac{|T_p-\tau|}{T_p}\right) \tag{12}$$

This ambiguity function is described in **Figure 11** with $N = 17$[1]. The increase of the number N of subchannels causes a decrease of the mainlobe size in the Doppler domain but does not change the mainlobe size in the delay domain. We will see that the choice of the line vector $[a_1, \cdots, a_N]$ with $a_i \in \{0,1\}$ is important and is managed by the goals of the application. We present in this chapter the case of OFDM waveform design for range ambiguity cancellation.

[1] In this case, the OFDM is not generated with an iFFT but with a inverse digital Fourier transform (iDFT).

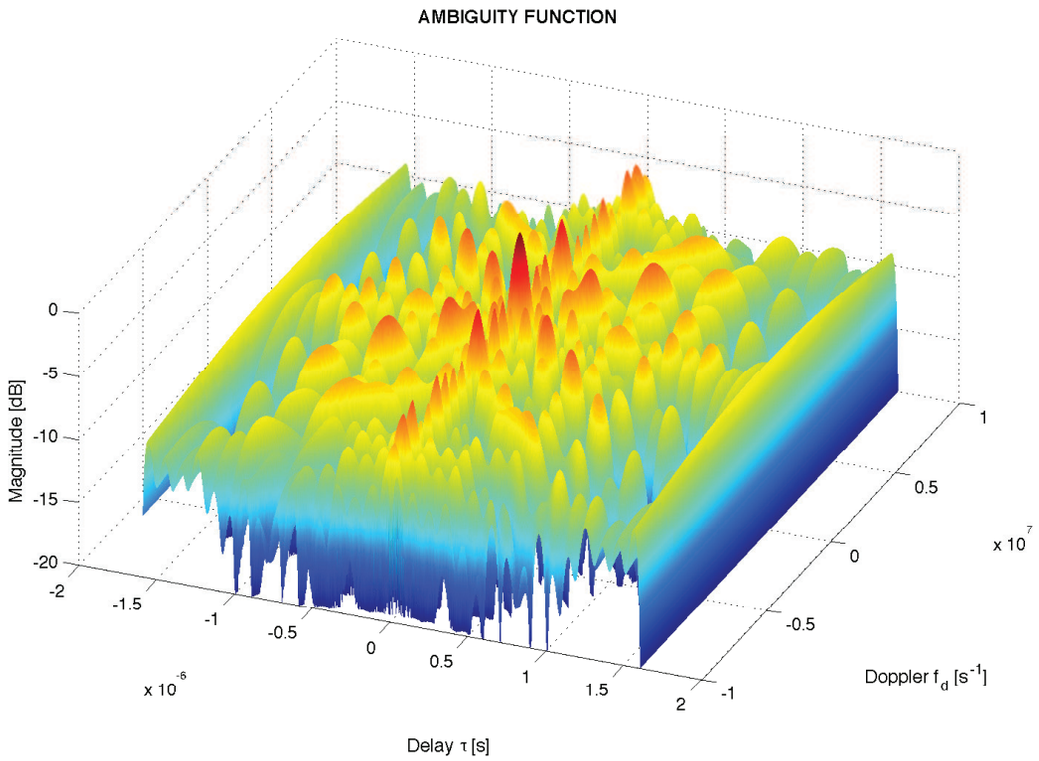

Figure 11. OFDM ambiguity function.

But, before designing the waveform for this task, the OFDM signal has to be characterised regarding the range and azimuth resolutions.

4.1. SAR OFDM signal

The OFDM signal expressed in Eq. (11) has a bandwidth per subchannel equal to $1/T_p$, the inverse of the rectangular pulse time duration. The OFDM signal is composed of N orthogonal subchannels, its total -3 dB bandwidth when all the a_i are set to one is $B = N/T_p$. If $N = KT_p^2$, where K is the frequency slope of the chirp given in Eq. (1), the range resolution of the OFDM signal is same as the chirp one and is given by Eq. (3). The compression and the range resolution driven by the parameter K with the chirp are driven by the parameter N with the OFDM. In both signal cases, the increase of the parameter increases the signal bandwidth and the range resolution.

Considering a single ground scatterer, as in Eq. (2), the range compressed OFDM signal is obtained after the matched filter. With the RF transposition of the baseband signal expressed in Eq. (11) at the frequency f_c, the compressed signal is

$$s_{rc}(t) = A_0^2 \sigma T_p \exp\left(-i2\pi f_c \frac{2R}{c}\right) \frac{1}{N} \sum_{i=1}^{N} \sum_{j=1}^{N} a_i a_j^* \exp\left(i2\pi \left(f_j t - f_i \frac{2R}{c}\right)\right) \operatorname{sinc}\left(f_i - f_j\right) T_p \tag{13}$$

http://dx.doi.org/10.5772/intechopen.71300

With a full OFDM signal, that is, $\forall i\ a_i = 1$, the pulse compression processing amplifies the SNR by a factor BT_p, as the chirp case does and the SNR is also given by Eq. (4).

As previously mentioned, one of the benefits of the OFDM signal is the spectrum flexibility. The question is then what appends if some a_i are null? In the simple case, where the null subchannels are on the edge of the OFDM spectrum, the signal bandwidth is proportional to the number N_a of active subchannels and the range resolution is

$$\delta_{rg} = \frac{cT_p}{2N_a} = \frac{c}{2B}\frac{N}{N_a} \geq \frac{c}{2B} \tag{14}$$

To obtain the minimal range resolution, active subchannels on the edge of the spectrum are obviously required. The question is now to know if it is possible to create holes in the spectrum without decreasing the range resolution. **Figure 12** gives results in two cases, with $N = 65$.

On **Figure 12a**, the range resolution is plotted versus the number of null subchannels in the middle of the spectrum. When this number of null subchannels is equal to zero, all the subchannels are active and the range resolution is the optimal one given by Eq. (3). With a number of null subchannels lower than 25, the range solution remains the optimal one whereas only 40 % of the subchannels are active. On **Figure 12b**, only two subchannels are active and the range resolution is plotted versus the number of null subchannels between these two active subchannels. When the number of null subchannels between the two active subchannels is equal to zero, the range resolution is given by Eq. (14) with $N_a = 2$. When the number of null subchannels between the two active subchannels increases, the resolution first decreases and secondly increases near the range resolution given by Eq. (14) with $N_a = 2$. Excessive increase of the size of the hole in the spectrum does not allow to keep the minimal range resolution given by the full bandwidth use.

We can conclude that if all the spectrum cannot be used, the OFDM design solution is to keep active the subchannels on the edge of the spectrum and to allow relative small hole within the

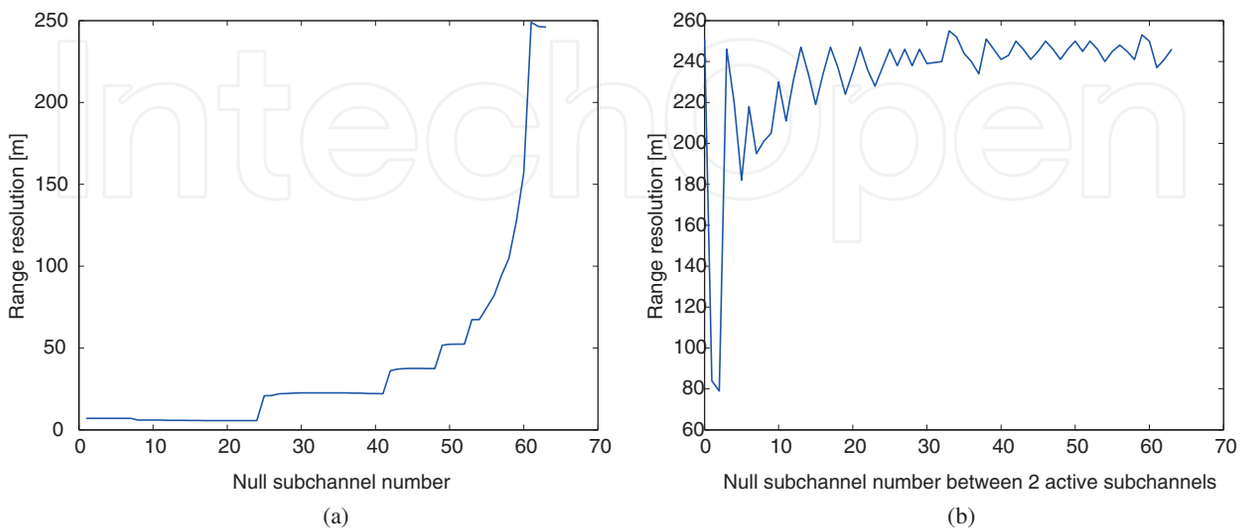

Figure 12. Range resolution versus active subchannels in OFDM signal.

spectrum. This strategy ensures an optimal range resolution. To retain the SNR in Eq. (4), the amplitude A_0 has to be scale to ensure a transmitting power independent of N_a.

4.2. Range ambiguity

The range ambiguity is well-known and studied in radar system [18]. This drawback mainly appears with high wide swath in satellite configuration and results from trade-off between high and low PRF. On the one hand, high PRF induces azimuth ambiguities while reducing the range ambiguities; on the other hand, low PRF induces range ambiguities while reducing the azimuth ambiguities. For example, let PRF_0 be the proper PRF, as shown in **Figure 13**. This PRF is set up to have the maximum swath width without ambiguities. In this case, a scatterer located far out the swath is well imaged as seen in **Figure 14a**.

If the PRF is larger than PRF_0, the scatterer becomes ambiguous as shown in **Figure 14b** and it is then considered as interference. The signal focusing also fails to operate along the azimuth axis and defocusing phenomenon occurs. A scatterer appears in the image at a range andazimuth where there is no scatterer.

The idea of range ambiguity suppression by alternating up and down chirp modulation is often discussed since it is obvious and easy to implement [19]. The goal is to keep a high PRF and to alternate waveforms with cross-correlation values as low as possible. With two different waveforms, the size of the unambiguous delay window is then multiplied by two, compared to the size obtained with the same PRF and with only one waveform. The unambiguous region can then be extended to the overall observed scene. As shown in **Figure 14c**, obtained with up and down chirp modulation, the scatterer is further well localised, as in the left unambiguous image, but a ghost appears due to the finite cross-correlation rejection values, roughly equal to 20 dB. Flexibility of the waveform is then required to improve the cross-correlation properties

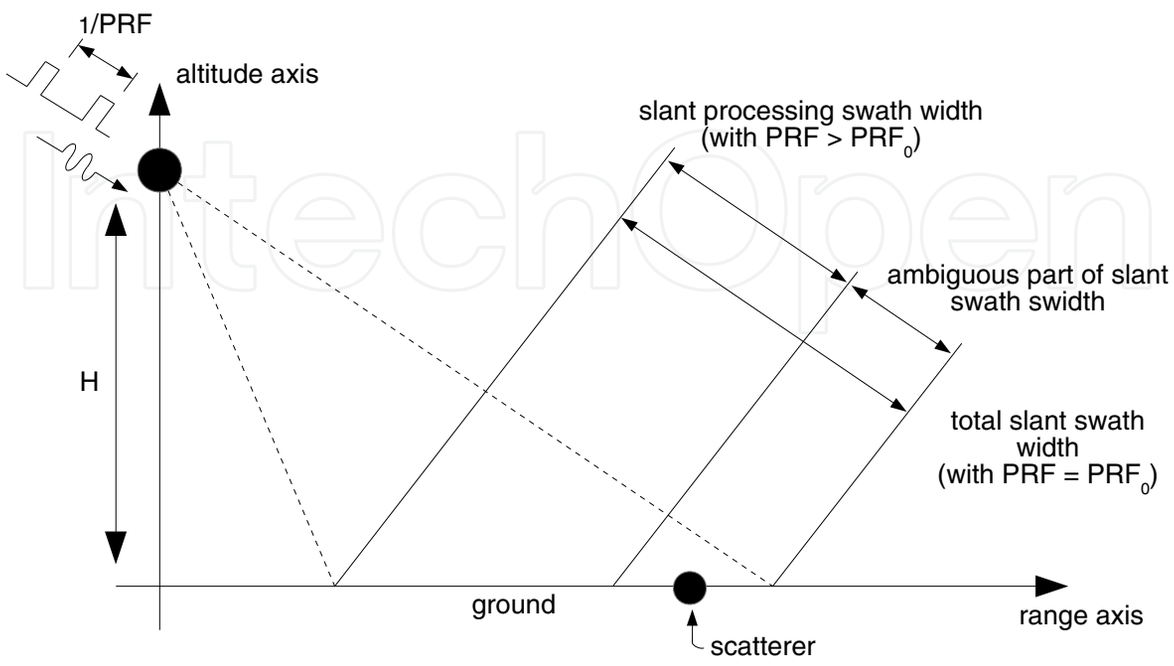

Figure 13. SAR imaging slant geometry taking range ambiguity into account.

http://dx.doi.org/10.5772/intechopen.71300

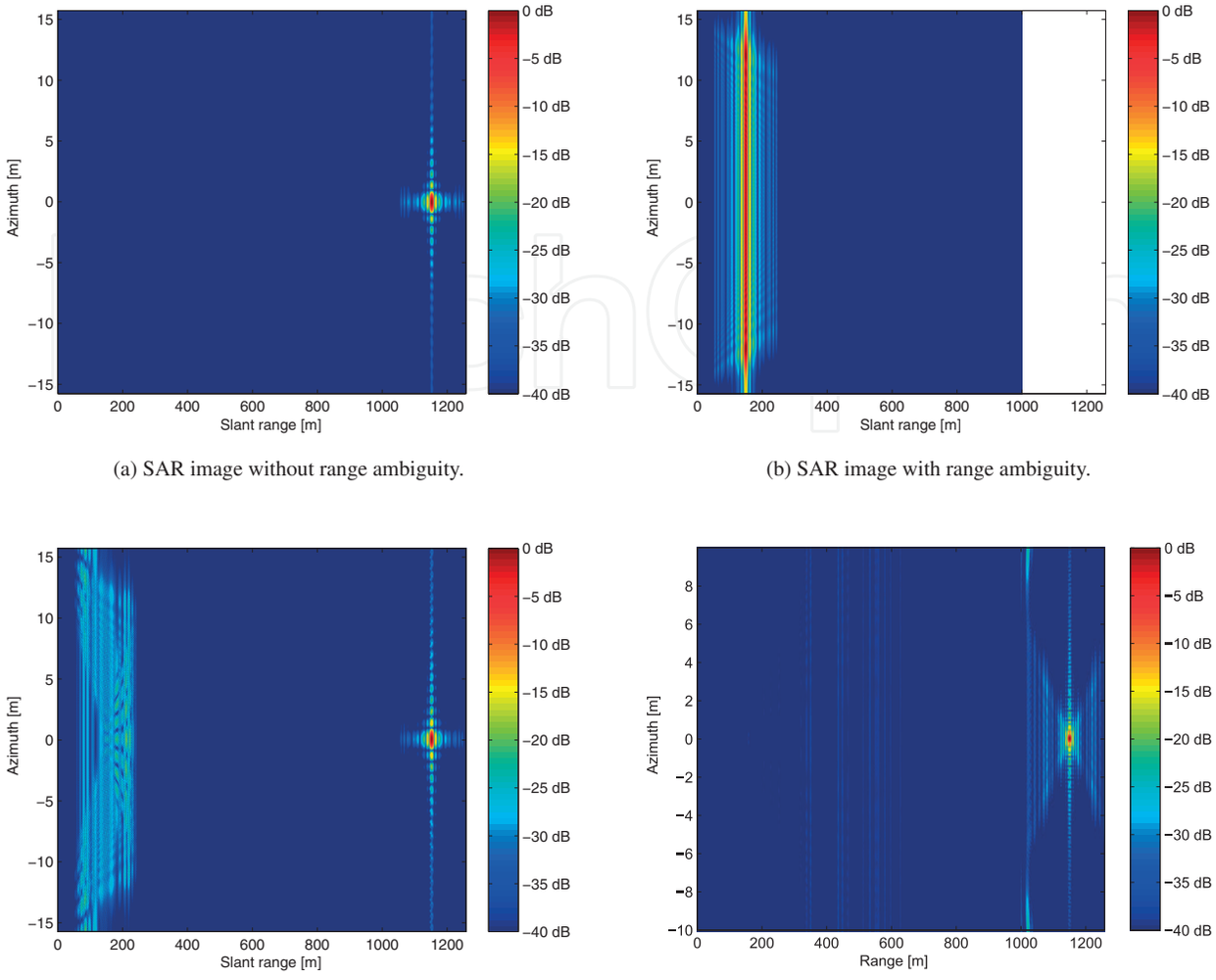

(a) SAR image without range ambiguity.

(b) SAR image with range ambiguity.

(c) SAR image with up and down chirp range ambiguity correction.

(d) SAR image with OFDM range ambiguity correction.

Figure 14. SAR images describing range ambiguity effects and a cancellation of them.

and to reduce the ghost level. The subchannel turning off and turning on capability of the OFDM offers this flexibility.

4.3. OFDM waveform design strategy

To cancel or reduce the range ambiguity phenomenon, we need multiple orthogonal signals or signals with good cross-correlation properties. It is now straightforward that OFDM is a good candidate to ensure this task: it is easy to create orthogonal signals using holes in the OFDM spectrum and at the same time to keep optimal range resolution for SAR applications. We provide an OFDM waveform design in the case of two generated signals, but the method can be extended to a larger number of orthogonal signals.

4.3.1. Signal requirements

To simplify the SAR imaging signal processing, the two signals must have the same characteristics: same carrier frequency, same subchannel frequency and same bandwidth.

The orthogonality of the OFDM spectrum simplify the generation of two orthogonal waveforms. Let $J = \{1, \cdots, N\}$ be the set of indexes of subchannels and two subsets J_a and J_b corresponding to the active subchannels of the signals. If $J_a \subset J$ is the set of active subchannels of the first OFDM signal, that is, $\forall i \in J_a \; a_i = 1$ and $\forall i \notin J_a \; a_i = 0$, then $J_b = J \setminus J_a$ is the set of active subchannels of the second OFDM signal. The orthogonality does not mean that the cross-correlation, given by Eq. (12) with $a_j = b_j = 1 - a_j$ and $\nu = 0$, is equal to zero for all the delay τ. This orthogonality is guaranteed when $\tau = \nu = 0$ and then we obtained easily $\chi_{a,b}(0,0) = 0$ with OFDM signals. However, this orthogonality is not enough to ensure good ambiguity rejection, the maximal relative cross-correlation amplitude should also be taken into account to optimise the signal waveform. This relative cross-correlation amplitude is defined as

$$\Delta\chi(a) = \max_{\tau} \frac{|\chi_{a,b}(\tau, 0)|}{|\chi_{a,a}(0,0)|} \tag{15}$$

and it is a function of a only, because b is completely determined by a.

To ensure optimal range resolution, the subchannels on the edge of the spectrum have to be active for both OFDM signals. However, to keep the orthogonality property, if a subchannel is active in one signal, it should be inactive in the other one. It has been proposed to set $a_1 = a_{N-1} = 1$ and $a_2 = a_N = 0$ in one OFDM signal and $b_2 = b_N = 1$ and $b_1 = b_{N-1} = 0$ in the other one [20]. The range resolution given in Eq. (14) becomes

$$\delta_{rg} = \frac{c}{2B}\left(1 + \frac{1}{N-1}\right) \tag{16}$$

which can be approximated by Eq. (3) when $N \gg 1$.

4.3.2. Optimisation strategy

The objective is to provide high-resolution SAR image. We have introduced two image quality parameters, the ISLR and PSLR, and we have added another parameter, the maximal relative cross-correlation amplitude in Eq. (15).

For spectrum equilibrium reason, N is odd and the subchannel in the middle is set to 0 in all the OFDM signals. Four other subchannels, two at each end of the spectrum, are fixed for range resolution reason. Then, it remains to allocate $N - 5$ subchannels in two OFDM signals. To have equal number of active subchannels per OFDM signal, each signal will have $(N-5)/2$ active subchannels and $(N-5)/2$ null subchannels. One have to choose $(N-5)/2$ active subchannels between $N - 5$ ones and the number of possible couples of OFDM signals are

$$N_{\text{couple}} = \frac{1}{2}\frac{(N-5)!}{\left(\frac{N-5}{2}!\right)^2} \tag{17}$$

With $N = 13$, the number of couples is 35. This low number allows exhaustive performance comparison to find the best couple. However, with higher number of subchannels, allowing higher design flexibility, the exhaustive search of the optimal couple solution becomes

unfeasible. For example, the value $N = 65$ leads to around 60 peta possible couples. To solve this search problem, genetic algorithm has been proposed [21]. This algorithm is based on a population of couple of OFDM signals iteratively modified to converge to the best couple solution. A fitness function is used to evaluate the performance of each couple and it is defined by

$$\psi(a) = \sum_{i=1}^{3} \alpha_i \frac{|\phi_i(a) - \phi_{i,0}|}{\phi_{i,0}} \tag{18}$$

where α_i is the weighting coefficient related to the objective function $\phi_i(a)$, which is equal to the PSLR given by Eq. (9) for $i = 1$, to the ISLR given by Eq. (10) for $i = 2$ and it is equal to the relative cross-correlation amplitude given by Eq. (15) for $i = 3$. The value of the objective functions is normalised by the reference values $\phi_{i,0}$ equal to or lower than $\min_a \phi_i(a)$.

The genetic algorithm is composed of five steps:

1. *Initialisation.* The first population of couples is randomly chosen. It is called the first generation;
2. *Evaluation.* The fitness function is calculated for each couple of the population;
3. *Selection.* It is a roulette-wheel selection and the selected couples are retained for the next generation. The selection is based on the value of the fitness function. The couples with high fitness function values are more likely to be selected for the next generation;
4. *Mutation.* Each selected couple is modified with a specific mutation probability. It means that each element of the vector a has the specific mutation probability to have its value changed;
5. *End condition.* The algorithm stops when the number of desired generations is reached, otherwise a new cycle of evaluation, selection and mutation starts. As the aim of the genetic algorithm is not to search for the all possible solutions, the ending condition limits the searching sub-space dimension by defining the expected number of generations.

To ensure the convergence of the algorithm to a local optimum, the couple with the lowest value of the fitness function in one generation is added unchanged to the next generation, that is, without mutation.

4.4. Simulation results

Although the range ambiguity mainly appears with high wide swath in satellite configuration, we consider an airborne configuration to evaluate the performance of the SAR imaging system in reasonable time. High value of the PRF is then chosen to increase the ambiguity phenomena. The carrier frequency of the transmitted signal is $f_c = 6$ GHz, the -3 dB signal bandwidth is 20 MHz and the number of subchannels of the OFDM signal is $N = 65$. The radar pulse length is $T_p = 3.25$ μs and the azimuth aperture angle is $\beta_{az} = 14.44^\circ$. The imaging system is located at a height $H = 3678$ m from the ground with an incidence angle $\alpha_e = 43.66^\circ$ is 1258 m whereas the PRF is 26.92 kHz, which leads to a unambiguous slant swath of 1000 m. This configuration

leads to an ambiguous configuration illustrated in **Figure 14**. The mutation parameter of the genetic algorithm is 20%, which ensures the search of a new solution close to the ones already found. The simulations are performed with the reference value $\phi_{i,0}$ given in **Table 3** and the weighting coefficients α_i are set to 1.

Figure 15 gives the lowest value of the fitness function for each generation. The genetic algorithm is applied five times to produce five optimised couples. The lowest value of the fitness function becomes quite flat after 15 iterations. We can conclude that this number of generation is enough to ensure a good optimised couple and **Table 3** gives the value of the objective function for each optimised couple. This table shows that the OFDM optimised signals outperform the chirp signals for all objective functions. **Figure 14d** shows the SAR

Optimisation	**PSLR [dB]**	**ISLR [dB]**	$\Delta\chi$ **[dB]**
#1	−18.5	−43.6	−11.3
#2	−18.5	−43.6	−11.4
#3	−18.5	−43.5	−11.6
#4	−18.5	−43.6	−11.0
#5	−18.3	−43.4	−12.1
Full OFDM	−16.4	−48.1	
Chirp couple	−13.9	−40.8	−9.2
$\phi_{i,0}$	−20	−48	−14

Table 3. PSLR, ISLR and $\Delta\chi$ for the different OFDM optimised couples (#1–#5) and a comparison with others transmitted signals.

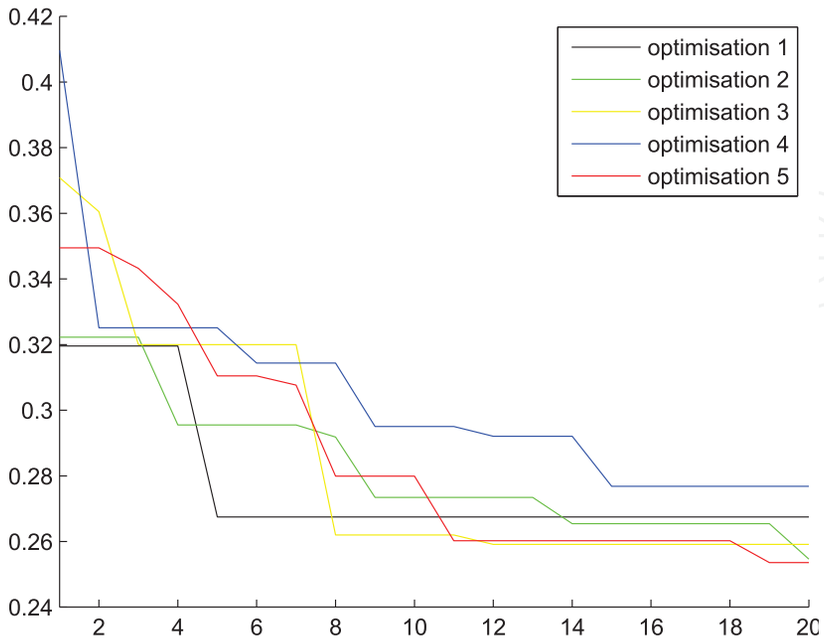

Figure 15. Objective function versus the generation number for 5 optimisation procedures.

image results with OFDM signals where the ghost has been largely reduced compared to **Figure 14c** obtained with chirp signal.

4.5. Discussion

The OFDM signals offer a good image quality improvement. The simulations are performed with $\forall i\ \alpha_i = 1$, which means that no priority is given to the objective function. Depending on the SAR application, priorities can be easily introduced to emphasis the desired parameter. We also focus on configurations with two OFDM signals. As mentioned, more than two signals with good cross-correlation properties can be generated with OFDM waveforms, which is not possible with the chirp signals. However, the OFDM signal has a main drawback that is not considered in this chapter: it has a high peak-to-average power ratio (PAPR). Two solutions can be provided. The first one consists to introduce a fourth objective function in Eq. (18) that takes into account the PAPR. The couple of the OFDM signals given by the genetic algorithm will minimise the PSLR, the ISLR, the cross-correlation amplitude and the PAPR. The other solution is to use complex symbols instead of 1, that is, the active subchannels are such that $a_i = e^{i\theta_i}$. The angle θ_i can also be introduced as a parameter to optimise in the genetic algorithm but random values lead high PAPR reductions [17].

5. MIMO OFDM SAR extension

As the previous procedure makes possible to set up orthogonal signals through the OFDM modulation, we propose to achieve SAR images in MIMO configuration. Some artefacts, that appear in MIMO SAR images, are due to the fact that the up- and down-modulated chirps do not provide the lowest cross-correlation level. Thus, we are interested to use OFDM signals for SAR applications in a MIMO context. The optimised OFDM pair provided by the optimisation procedure is then used in a MIMO configuration composed of two transmitting and receiving antennas.

As previously done in Section 4, an optimised OFDM couple composed of 65 subchannels are obtained with the use of the genetic algorithm. These OFDM signals are then associated with the SAR MIMO method exposed in Section 3. The results thus obtained are compared with those obtained in the case of the use of the MIMO SAR method with chirps signals and those obtained in the case of the use of an SISO configuration. The geometric configuration described in Section 3 is the same for this comparison and a metallic trihedral placed in the region of interest is considered to be at a 3.53 m range, that is, 5 m along the line-of-sight axis. In the two reference configurations without noise, the images shown in **Figure 16a** for the SISO SAR configuration and **Figure 16c** for the SAR MIMO configuration using transmitted chirps are obtained.

By analysing the SAR MIMO configuration with the chirps signals, the artefact appears along the azimuth axis on both sides of the metallic trihedral and the maximum level of this artefact is equal to -27 dB. The position of these phenomena is related to the position of the transmitting and receiving antennas. In our case, the artefacts are located at the coordinates

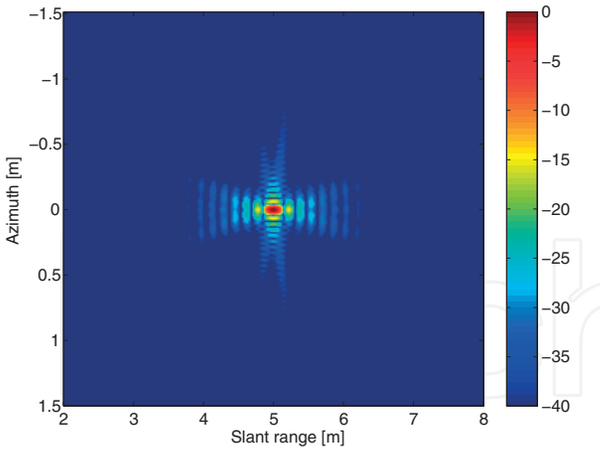

(a) SISO SAR image.

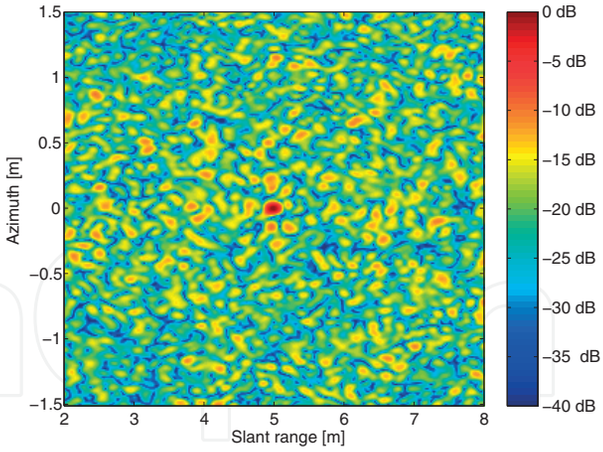

(b) SISO SAR image with noise.

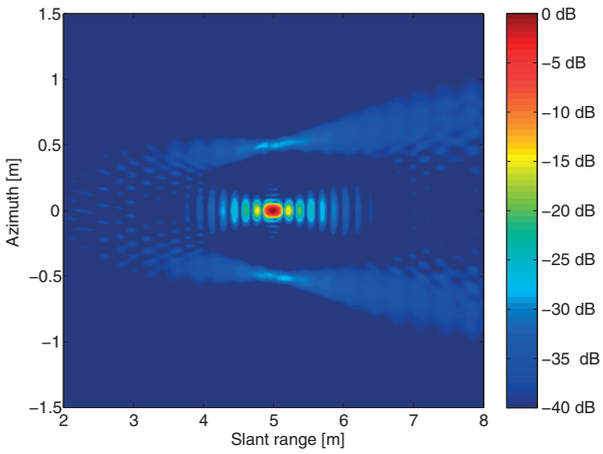

(c)

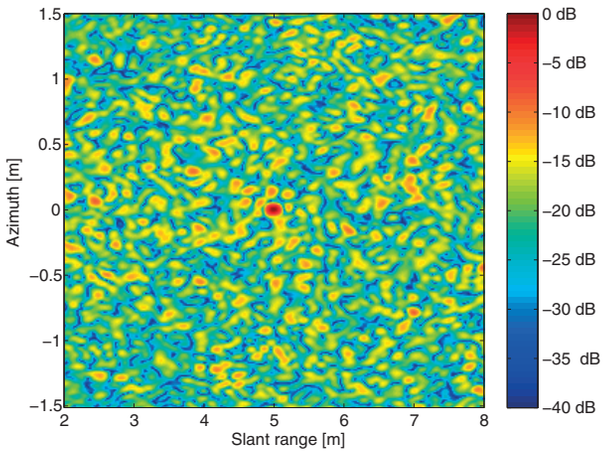

(d) MIMO SAR image with chirp transmitted waveforms and noise.

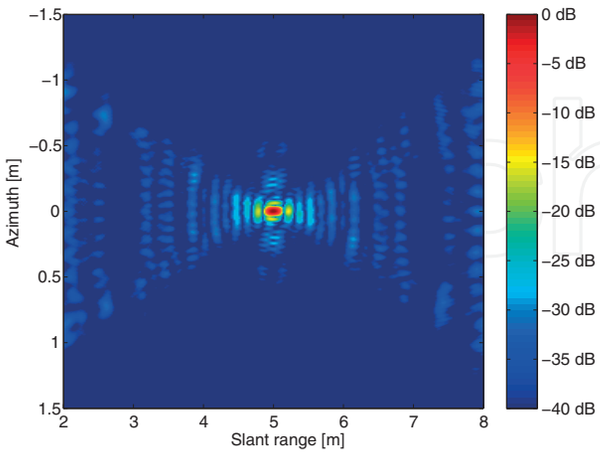

(e) MIMO SAR image with OFDM transmitted waveforms.

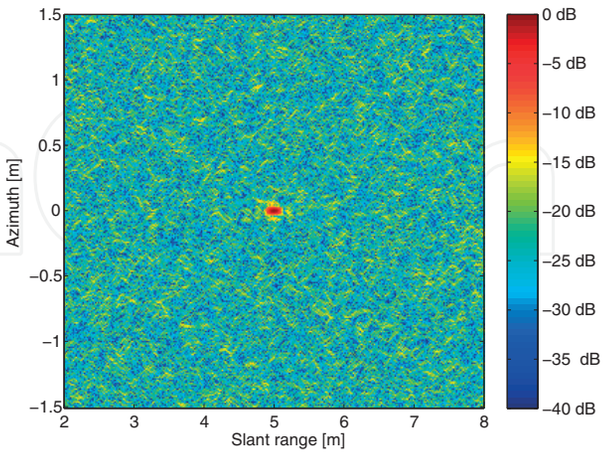

(f) MIMO SAR image with OFDM transmitted waveforms and noise.

Figure 16. SAR images provided by three different configurations without and with noise.

	Azimuth resolution (m)	PSLR (dB)	ISLR (dB)	PSLR (dB)	ISLR (dB)
		Without noise		With noise	
SISO	0.056	−13.8	−31	−9.5	−11.7
chirps MIMO	0.048	−14.2	−31	−11.2	−14.4
OFDM MIMO	0.037	−14.9	−32.4	−12.0	−17.3

Table 4. Simulation results of the azimuth resolution, PSLR and ISLR for different SAR configuration.

($x = 0$ m, $y = 0.56$ m) and ($x = 0$ m, $y = -0.56$ m). In the case of the MIMO OFDM SAR configuration, which is shown in **Figure 16e**, the azimuth artefacts have been largely reduced. Moreover, we are able to produce the similar results by adding noise resulting in a −30 dB SNR for the received signal. The corresponding SAR images are exhibited in **Figure 16b, d, f**. The imagery parameters are obtained and summarised in **Table 4**.

The azimuth resolution equal to 0.037 m is obtained. The azimuth resolution is improved by using the MIMO configuration together with the OFDM signals. However, the values of the other parameters, ISLR and PSLR, are modified. These improvements are due to the use of optimised OFDM transmitted signals. In the context of SAR MIMO imaging, the use of OFDM signals optimised in transmission makes it possible to greatly reduce the phantom phenomenon in azimuth. Moreover, in the case of a noisy environment, the use of OFDM signals coupled with MIMO techniques induces a stronger resistance to noise.

6. Conclusion

Based on the concepts from digital communications, this chapter discusses the improvement of the SAR processing performances provided by a MIMO-type configuration on the one hand and an OFDM-type waveform on the other hand. In order to illustrate the benefits of these approaches, we address some performances as the system robustness of SAR system, the azimuth resolution of SAR images and the range ambiguity of SAR processing.

First, the principle of SAR imaging is shown. The performances under study, which are achieved for the SISO SAR configuration with the chirp waveform, are also detailed. We assess the improvements that we apply, through differents parameters as PSLR, ISLR and azimuth resolution. These parameters make possible to describe the capabilities of system configuration and waveform design to improve the SAR images. The section about the MIMO configuration analysis describes the procedure for a coherent system regarding the geometric situation. Based on the backprojection SAR processing, some simulations achieve a coherent addition of SAR images to each other that induces an increase in noise resistance. The described procedure is validated by the use of an experimental system. This study of the receiver part of the MIMO

SAR shows us the possibility of improving the azimuth resolution and the robustness of the imaging system by using a MIMO configuration. The next section deals with the use of OFDM signals to solve a limitation related to range ambiguity phenomena. This method is then validated by simulation using a pair of chirps (up- and down-modulated chirps). Nevertheless, these transmitted signals are not totally orthogonal artefacts appear in the SAR image along the azimuth axis. Thus, a procedure is proposed in order to determine the optimum OFDM signal couple to solve the ambiguity in range and at the same time to reduce the presence of artefacts in the final image. An optimization procedure based on a genetic algorithm is used and validated for 65 subchannels. Finally, the use of the OFDM signals is proposed with the MIMO concept. In the same way as for range ambiguity, the MIMO SAR focusing methods are all based on the use of matched filters in range. By using the optimal OFDM couple determined to solve the range ambiguity, it is possible to improve the SAR image.

This chapter indicates a number of avenues for future research directions and gives first answers to the problem we investigate. For example, some lines of research seem interesting to explore. It would be interesting to increase the number of transmitting or receiving antennas in order to increase the robustness of the radar system against noise. Another application of OFDM for SAR imaging is the use of OFDM signals coupled with polarimetry because it is often necessary to increase the PRF to make a second acquisition by changing the transmitted polarisation.

Author details

Stéphane Méric* and Jean-Yves Baudais

*Address all correspondence to: stephane.meric@insa-rennes.fr

Institute of Electronics and Telecommunications of Rennes, Rennes, France

References

[1] Cumming IG, Wong FH. Digital Processing of Synthetic Aperture Radar Data. Norwood, USA: Artech House Inc.; 2005

[2] Richards MA, Scheer J, Holm WA. Principles of Modern Radar: Basic Principles. Rayleigh, USA: SciTech Publishing Inc; 2010

[3] Soumekh M. Synthetic Aperture Radar Signal Processing. New-York, USA: Wiley-Interscience Inc.; 2004

[4] Chevalier FL. Application to radar. In: Principles of Radar and Sonar Signal Processing. Norwood, USA: Artech House Inc.; 2005. pp. 39-106

[5] Klare J, Saalmann O, Wilden H, Brenner AR. First experimental results with the imaging MIMO radar MIRA-CLE X. In: European Conference on Synthetic Aperture Radar. 2010. pp. 374-377

[6] Martínez A, Marchand JL. SAR Image quality assessment. Revista de Teledetección. 1993 Nov;**1993**(2):1-7

[7] Levanon N, Mozeson E. Radar Signals. New-York, USA: Wiley-interscience Inc.; 1999

[8] Klare J, Saalmann O, Wilden H, Brenner A. Environmental monitoring with the imaging MIMO radars MIRA-CLE and MIRA-CLE X. In: IEEE International Geoscience and Remote Sensing Symposium. 2010. pp. 3781-3784

[9] Ender JHG, Klare J. System architectures and algorithms for radar imaging by MIMO-SAR. In: Radar Conference. Pasadena, CA, USA. 2009. pp. 1-6

[10] Li SF, Chen J, Zhang LQ, Zhou YQ. Application of complete complementary sequence in orthogonal MIMO SAR system. Progress in Electromagnetics Research C. 2010;**13**:51-66

[11] Li J, Zheng X, Stoica P. MIMO SAR imaging: Signal synthesis and receiver design. In: International Workshop on Computational Advances in Multi-Sensor Adaptive Processing. 2007. pp. 89-92

[12] Riché V, Méric S, Pottier É. Study of receiver design in a MIMO SAR configuration. International Journal of Microwave and Wireless Technologies. 2012;**4**(3):335-339

[13] Kauffman K, Raquet J, Morton Y, Garmatyuk D. Enhanced feature detection and tracking algorithm for UWB-OFDM SAR navigation. National Aerospace and Electronics Conference. 2011:261-269

[14] Hossain MA, Elshafiey I, Alkanhal MA, Mabrouk A. Anti-jamming capabilities of UWB-OFDM SAR. In: European Radar Conference. Manchester, UK. 2011. pp. 313-316

[15] Garmatyuk D, Brenneman M. Adaptive multicarrier OFDM SAR signal processing. IEEE Transactions on Geoscience and Remote Sensing. 2011 Oct;**49**(10):3780-3790

[16] Liu X, Liu Y, Wang X, Zhou J. Application of communication OFDM waveform to SAR imaging. In: Radar Conference. 2017. pp. 1757-1760

[17] Baudais JY, Méric S, Riché V, Pottier É. MIMO-OFDM signal optimization for SAR imaging radar. EURASIP Journal on Advances in Signal Processing. 2016;**2016**:1-11

[18] Curlander JC, McDonough RC. Synthetic aperture radar: Systems and signal processing. New-York, USA: Wiley-Interscience Inc.; 1991

[19] Mittermayer J, Martínez JM. Analysis of range ambiguity suppression in SAR by up and down chirp modulation for point and distributed targets. In: IEEE Internationnal Geoscience and Remote Sensing Symposium. Toulouse, France. 2003. pp. 4077-4079

[20] Riché V, Méric S, Baudais JY, Pottier É. OFDM signal design for range ambiguity suppression in SAR configuration. In: IEEE International Geoscience and Remote Sensing Symposium. Munich, Germany. 2012. pp. 2156-2159

[21] Riché V, Méric S, Baudais JY, Pottier É. Optimization of OFDM SAR signals for range ambiguity suppression. In: European Radar Conference. Amsterdam, Netherlands. 2012. pp. 278-281

IntechOpen